Technium Vol. 4, No. 9 pp.23-46 (2022)
ISSN: 2668-778X
www.techniumscience.com

Investigation on torque ripple minimization in switched reluctance motor by using different techniques associated with TSF taking into account of magnetic saturation effects

SISSINVOU Manassé [1], YOUMSSI André [2], KENMOE FANKEM E. D [3], GUIDKAYA Golam [4].
sissinvou@gmail.com ayoumssi@yahoo.fr fankeme@yahoo.fr golam.guidkaya@ yahoo.fr

[1]PhD student at Doctoral Training PAI, University of Ngaoundéré -Cameroon.
[2]IEEE Transactions and Elsevier Senior Reviewer. Associate Professor, University Institute of Technology, University of Ngaoundéré -Cameroon.
[3] Associate Professor, Faculty of Sciences, University of Ngaoundéré – Cameroon
[4]Assistant lecturer, Faculty of Sciences, University of Ngaoundéré – Cameroon
Corresponding author : GUIDKAYA Golam golam.guidkaya@ yahoo.fr

Abstract:

In this work, three control techniques of minimization of torque ripple in SRM are proposed and compared to the classical control technic names as Hysteresis control proposed in [1]. The principle of these methods is based on the Torque Sharing Function (TSF) fixing the reference torque in each phase. In the literature review, the classical method used in the reduction of torque ripples in SRM is the TSF-Hysteresis Controller (TSF-H). The first proposed method is the TSF-Predictive control (TSF-P), here the objective is to find the voltage to be applied to the machine minimizing the error of the current through a prediction algorithm on the supply current. The second proposed method is the sliding mode control (TSF-SMC-PSO) whose parameters are optimized by the particle swarm algorithm (PSO). Finally, the third proposed method is the sliding mode controller whose parameters are optimized by fuzzy logic controller (TSF-SMFC). The finite element method (FEM) through the magnetic field calculation software FEMM was used to calculate the flux and torque in static system and to take into account magnetic saturation circuit of the SRM. The results obtained show that the TSF-SMC-PSO control methods have better performance compared to the other proposed methods mentioned above.

Keywords. Switched Reluctance Motor, Torque Ripple Reduction, Torque Sharing Function, Predictive Control, Sliding Mode Control, Particle Swarm Optimization, Fuzzy Logic Control.

1. Introduction

Switched reluctance motors (SRMs) are widely used in many industrial applications like automotive field, aeronautics industry and renewable energies. Many researchers focus on this type of machine because of their advantages like simple construction and maintenance, low cost, good efficiency [2], no permanent magnets, no winding on rotor, high speed operation and high temperature handling capability [3], [4]. However, the drawback associated with SRM is high torque ripple leading to acoustic noise and vibration. The large torque ripple is due to high nonlinearity and discrete nature of torque production mechanism.

In the literature, several researchers have contributed to the minimization of torque ripples in SRM. To achieve this, two approaches are used, the geometrical approach which consists of modifying the shape of the rotor or stator of SRM in order to have positive impact on the torque; and the control approach which consists in using an adequate control technique to minimize torque ripples [5] [6] [4].

To overcome this problem, several control techniques have been proposed in the literature. The Torque Sharing Function (TSF) is an indirect torque control method widely used in the minimization of torque ripples [7]. In the TSF method, the total torque is individually distributed in each phase from predefined functions which try to generate a constant torque during the conduction and commutation of each phase [8] [9] [10]. There are several types of TSF such as exponential, cosine, cubic, and linear [11]. Classically, the reference torque can be defined using analytic expressions [12]. Moreover, to improve and reduce torque ripples in commutation zone, the authors in [13] propose the nonlinear logical TSF. This method takes into account not only the case where only one phase is supply, but also the case where two phases are simultaneously supply. The incoming phase current needs to be increasingly controlled and at the same time the outgoing phase current follows the opposite direction such that the torque sharing can easily be achieved with minimal overshoot. This method effectively reduces the torque ripples taking into account the saturation of the magnetic circuit. The use of the Iterative Learning Control (ILC) method for torque ripple reduction is proposed in [14], it allows to add a compensation current to the reference current in order to eliminate the torque error. In [15], phase current profiling method is used to minimize the torque ripples. This method is a combination of geometric modelling and control algorithm. The minimization is done in 3 steps, the first consists in modelling a symmetrical torque machine, the second finding the required current profile via the simulations and finally the third, finding the optimized profile. This method is effective because it takes into account the electrical nonlinearity and magnetic losses.

In this paper, several methods for minimizing torque ripples using the torque sharing function are proposed. The first method is based on predictive control, the reference torque profile is fixed using the torque sharing function (TSF), we named this method (TSF-P); the predicted current is obtained by carrying out the first order Euler discretization of the dynamics of phase currents (derivative of the current with respect to time). The latter being a function of the voltage supplied by the inverter; the supply voltage level of the inverter is chosen by an algorithm selection making it possible to obtain a minimum error between the reference current resulting from the TSF and the predicted current. The feasibility of this method is mainly due to the fact that the phases of SRM are supply independently unlike other electric machines. The second method also uses TSF associated with a sliding mode control whose parameters are optimized by the particle swarm algorithm that we have called (TSF-SMC-PSO). Classically, the control parameters of the SMC method are obtained by Lyapunov's function; however, the latter only gives the ranges of values of those parameters which the system is stable, unlike the PSO algorithm gives the optimal value of those parameters. The third method is the TSF associated with the sliding mode controller whose parameters are optimized by the fuzzy logic controller (TSF-SMFC). All these methods are compared to the classical method proposed in [1] (TSF-H method).

First, the finite element analysis was used to calculate static flux and static torque of SRM taking into account of the magnetic saturation using FEMM software (Finite Elements Method Magnetics) driven by Matlab programming software. These data are then integrated into the Simulink model for studying the dynamic behaviour of SRM through the back electromotive force per speed unit, the incremental inductance and the static torque.

2. Structure of SRM

The SRM is characterized by its double salient poles and the windings are concentrated around the stator teeth while the rotor is without windings, which makes its structure simple and advantageous compared to other machines. The SRM studied is an 8/6 SRM with height (8) poles on stator and six poles on the rotor. The stator poles have four (4) phase windings for excitation. The magnetic problem is analyse using two dimensional finite element method (FEM) associated with Matlab software. Figure 1 shows a 2D cross section of the 8/6 SRM considered in the present study, and Table I shows the specifications of this 8/6 SRM and figure 2 present the magnetic flux distribution obtained through FEM software.

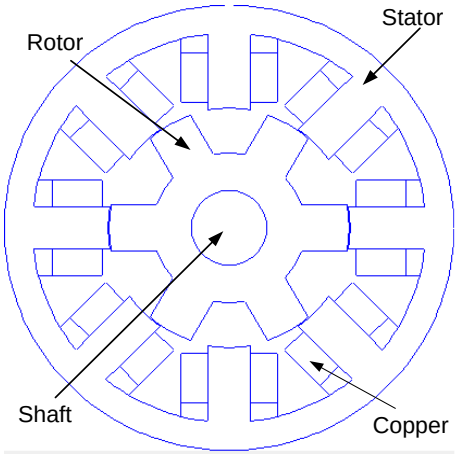

Figure 1: 2D Cross section of the studied 8/6 SRM

Table 1: Geometric Dimensions of the 8/6 SRM studied [16]

Number of stator poles, *Ns*	8
Number of rotor poles, *Nr*	6
Lamination outer radius (mm)	89.8
Stator yoke inner radius (mm)	78.4
Stator bore radius (mm)	48.18
Rotor outer radius (mm)	47.82
Rotor yoke outer radius (mm)	30.3
Rotor yoke inner radius (mm)	15
The pole arc of the stator (Deg)	20.2
The pole arc of the rotor (Deg)	22.5
Length of the stator laminations (mm)	151
Winding Number of turns per electric phase, N	176

Technium Vol. 4, No. 9 pp.23-46 (2022)
ISSN: 2668-778X
www.techniumscience.com

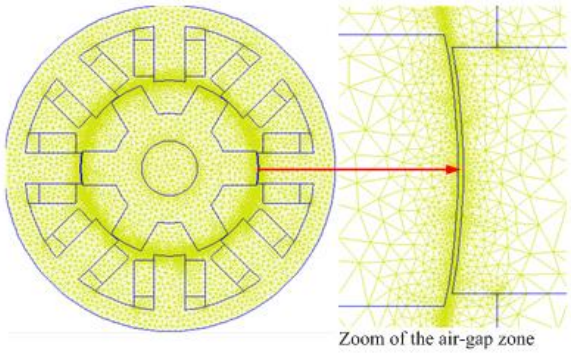

Figure 2: Mesh of 8/6 SRM by FEM

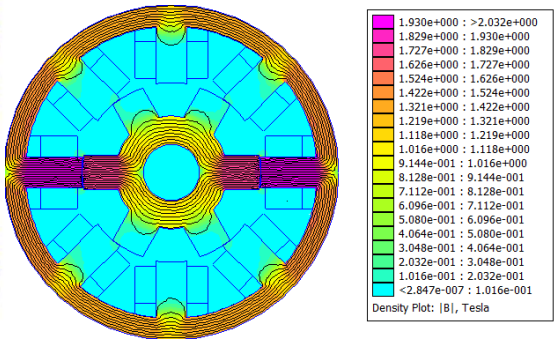

Figure 3: Magnetic flux distribution by FEM

3. Dynamic study of 8/6 SRM

To supply the SRM, one of the most important parts is modeling the power converter that can efficiently produce a desired output. Several researchers have investigated in the production of the control circuit of this type of machine [17] [18] [19]. The SRM is satisfied with a unidirectional power supply for each phase since the direction of the current has no influence on the sign of the torque produced. This current, must be established quickly, be maintained more or less constant, then decrease rapidly.

The dynamic model of the 8/6 SRM is governed by mathematical equations linking the electrical, mechanical and electromagnetic parameters [16]. The instantaneous voltage for each phase of SRM is given by the following equation

$$U_j = R_s i_j + \frac{d\psi_j(\theta,i_j)}{dt} \qquad (1)$$

The flux linkage in SRM is a nonlinear function of the rotor position and the motor current [20]. Therefore

$$U_j = R_s \mathrm{i_j} + \frac{\partial \psi_j(\theta,\mathrm{i_j})}{\partial \mathrm{i_j}} \frac{\partial \mathrm{i_j}}{\partial t} + \frac{\partial \psi_j(\theta,\mathrm{i_j})}{\partial \theta} \frac{\partial \theta}{\partial t} \qquad (2)$$

The dynamic mechanical equations is given as follow [16] :

$$\frac{\mathrm{d}\Omega}{\mathrm{dt}} = \frac{1}{J}(T_e - f_v\Omega - T_L) \qquad (3)$$

$$\frac{\partial \theta}{\partial t} = \Omega \qquad (4)$$

$$\mathrm{T_e} = \sum_{\mathrm{j=1}}^{4} T_j(\theta, i_j) \qquad (5)$$

4. Torque ripple minimization approach

4.1 TSF-Hysteresis (TSF-H)

The simple concept as well as the ease of application in torque control and the minimization of torque ripples in SRM, has allowed the TSF method to be strongly considered in research and industrial applications. In this method, the reference torque is distributed in different phases through predefined functions that try to keep the torque produced constant during the conduction of one phase and the commutation of each phase. Torque produced by the motor is obtained from the addition of the individual torque produced by each phase.

The generalized expression of TSF of j^{th} phase as a function of the rotor position is given by the following relation [21]:

$$f_j(\theta) = \begin{cases} 0, & 0 \le \theta \le \theta_{on} \\ f_{rise(\theta)}, & \theta_{on} \le \theta \le \theta_{on} + \theta_{ov} \\ 1, & \theta_{on} + \theta_{ov} \le \theta \le \theta_{off} \\ f_{fall(\theta)}, & \theta_{off} \le \theta \le \theta_{off} + \theta_{ov} \\ 0, & \theta_{off} + \theta_{ov} \le \theta \le \theta_{al} \end{cases} \quad (6)$$

Where $\boldsymbol{\theta_{on}}$ is starting angle, $\boldsymbol{\theta_{off}}$ the ending angle and $\boldsymbol{\theta_{ov}}$ the overlap angle of commutation.

The aligned position of rotor with stator pole of j^{th} phase is taken as reference angle. The reference torque for j^{th} phase will then be given as follows:

$$T_j^* = T^* f_j(\theta) \quad (7)$$

Where T^* the reference torque to be reached. During commutation, the commutation angle of phase j will share the reference torque with the outgoing phase $(j-1)$ and the incoming phase $(j+1)$. Thus for any TSF, the function $f_{fall(\theta)}$ is given by the following relation:

$$f_{fall(\theta)} = 1 - f_{rise(\theta - \theta_{off} + \theta_{on})}. \quad (8)$$

The rise function, $f_{rise(\theta)}$ and the fall function, $f_{fall(\theta)}$ are defined based on the TSFs employed in [14]. Table 2 shows the definition of the rise function, $f_{rise(\theta)}$ of each basic TSF.

Table 2. Basic definition of TSF [22]

TSF	$\boldsymbol{f_{rise(\theta)}}$
Linear	$\frac{\theta - \theta_{on}}{\theta_{ov}}$
Exponential	$1 - exp\left(-\frac{(\theta - \theta_{on})}{\theta_{ov}}\right)$
Cosine	$0.5 - 0.5cos\left(\frac{\pi(\theta - \theta_{on})}{\theta_{ov}}\right)$
Cubic	$\frac{3}{\theta_{ov}^2}(\theta - \theta_{on})^2 - \frac{2}{\theta_{ov}^3}(\theta - \theta_{on})^3$

Figure 4 shows the control block diagram of the conventional TSF controller associate with hysteresis control.

Technium Vol. 4, No. 9 pp.23-46 (2022)
ISSN: 2668-778X
www.techniumscience.com

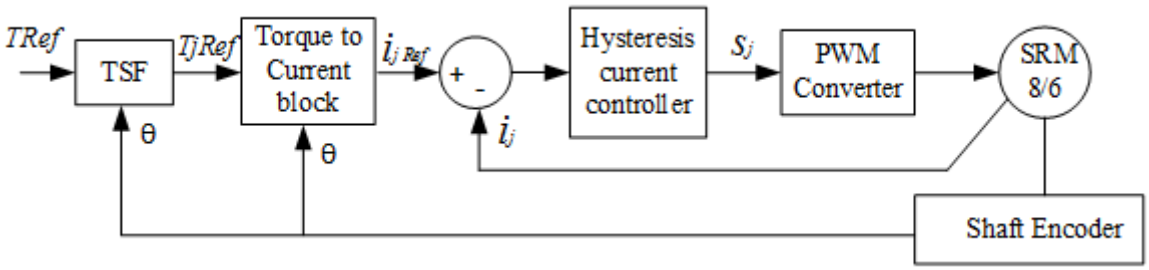

Figure 4 : Block diagram of TSF-Hysteresis control [1].

Torque is distributed individually in each phase as reference torque through the TSF block. These torques are then converted into command currents through a look-up table contained in the Torque to Current block. This block converts each reference torque into a reference current corresponding to each phase depending on the position of the rotor. Hysteresis controller can then be used to generate switching signals to the PWM converter which operates in DC.

4.2. *TSF-Predictive (TSF-P)*

The principle of this method is based on the association of an inverter with a predictive current controller. The trick of this technique is to apply a predictive control on the currents which are a function of the voltage levels of the inverter. The advantage of using multi-level inverter allows us to vary the current according to the voltage level provided by the inverter and therefore the torque. In other words, this technique takes into account the intermediate voltage levels unlike the hysteresis controller which has only two voltage levels, which limits its performance in minimizing torque ripples.

Torque ripples are very pronounced in the commutation zone than in the zone where a single phase conducts. This is mainly due to the variations of the two currents, i.e. the decrease in current i_j and the increase in current $i_{(j+1)}$. The current i_j decreases with the same supply voltage and the current $i_{(j+1)}$ also increases with the same supply voltage.

In this method, dynamic currents approach is used because its equation is simple and easy to manipulate, unlike the torque dynamics which involves second derivatives, which makes the calculations even more complex.

From equation (2), we compile the dynamic of current of each phase of SRM as follow:

$$\frac{\partial \mathrm{i_j}}{\partial t} = \left(\frac{\partial \psi_j(\theta,\mathrm{i_j})}{\partial \mathrm{i_j}}\right)^{-1}\left(\mathrm{U_j} - \mathrm{R_s i_j} - \frac{\partial \psi_j(\theta,\mathrm{i_j})}{\partial \theta}\,\Omega\right) \qquad (9)$$

Therefore, we must first discretize the dynamic of current on equation (9) using the numerical approach by Euler equation first order [23]. Discretize current is given on equation (10) where k is the discretization element. This allow us to manipulate the current element by element.

$$\frac{di_{jk}}{dt} = \frac{i_{j(k+1)} - i_{jk}}{T_s} \qquad (10)$$

Where i_{jk} is discretized current of j^{th} phase of the element k; $i_{j(\mathrm{k+1})}$ the future current of j^{th} phase of the element $(k+1)$ and $\mathrm{T_s}$ is the calculation step.

By substituting equation (10) into equation (9) we get:

$$\frac{i_{j(k+1)} - i_{jk}}{T_s} = \left(\frac{\partial \psi_{jk}(\theta,i_{jk})}{\partial i_{jk}}\right)^{-1}\left(U_{jk} - R_s i_{jk} - \frac{\partial \psi_{jk}(\theta,i_{jk})}{\partial \theta}\,\Omega\right) \qquad (11)$$

Finally, the future current $i_{j(k+1)}$ can be now express as follow

$$i_{j(k+1)} = i_{jk} + T_s \left(\frac{\partial \psi_{jk}(\theta, i_{jk})}{\partial i_{jk}}\right)^{-1} \left(U_{jk} - R_s i_{jk} - \frac{\partial \psi_{jk}(\theta, i_{jk})}{\partial \theta}\, \Omega\right) \quad (12)$$

The error current can therefore be evaluated according to equation (13):

$$\varepsilon_{jk} = i_{jref} - i_{j(k+1)} \quad (13)$$

Relation (12) shows that the future current $i_{j(k+1)}$ depends on the voltage U_{jk} provide by the inverter and the present current i_{jk}. The predictive control algorithm therefore evaluates the future currents $i_{j(k+1)}$ by filling all the voltage levels of the inverter U_{jk} in a calculation loop while evaluating the error current each time. The calculated error values are stored in an error vector ε. To determine the voltage to be used for supplying each phase, an algorithm selects among the voltage levels of the inverter, the voltage which gives a minimum current error ε_{jk}. Thus, the cost function can be expressed by the following relation:

$$C_f = i_{jref} - i_{j(k+1)} \quad (14)$$

The objective of the predictive current algorithm is to determine the value of the voltage to be applied on the SRM which minimizes the cost function C_f . We are therefore going to use a conventional inverter which provides three different voltage levels $(E, 0, -E)$, where E is the DC bus voltage supplying the inverter. The inverter voltage Selection Flowchart is presented on figure 5

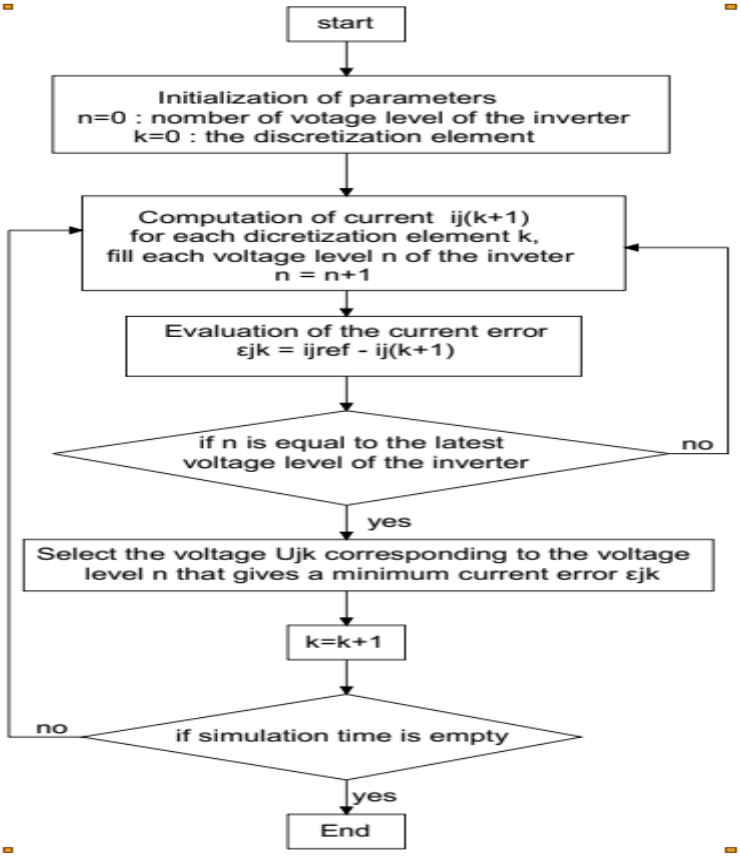

Figure 5: Inverter Voltage Selection Flowchart

Figure 6 shows the control block diagram of the proposed TSF Predictive control. The TSF block which individually distribute reference torque in each phase by using cosine mathematical function according to rotor position given by shaft encoder. In the output we have individual reference torque of each phase. The "Torque to current" block is used to convert individual reference torque obtained at the output of the TSF block into a reference current for each phase. The Predictive current controller block which is equipped with the current prediction algorithm provides the control signal to the converter minimizing the error between the reference current and the current estimated by the SRM.

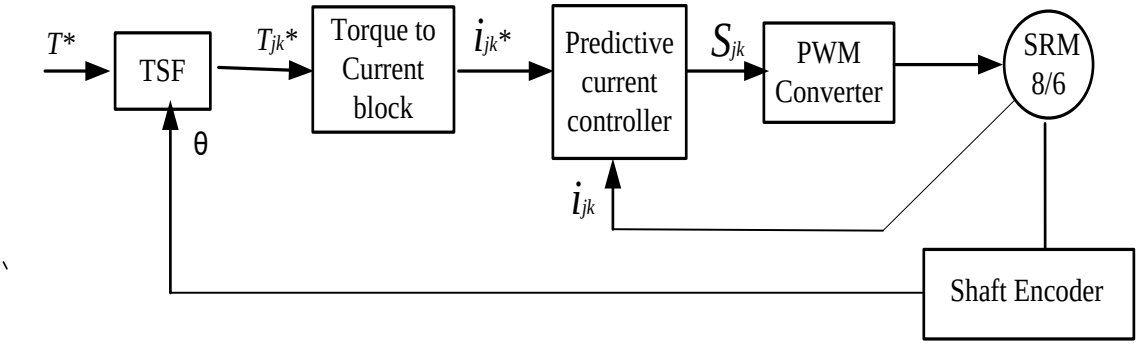

Figure 6 : Bloc diagram of TSF-Predictive Controller

4.2. TSF-Sliding Mode-PSO Control (TSF-SMC-PSO)

Variable structure of a systems in sliding mode have already been used by many authors in different control applications [24]. Variable structure of a systems consists of a set of continuous subsystems with appropriate switching logic. By consequence, control actions are discontinuous functions of states of a system, disturbances, and reference input. However, it is reported by many authors that the sliding mode in motion control has an advantage imposed by discontinuity of action control. By combining variable structure of a systems and Lyapunov's design approach, continuous control of sliding mode systems has been designed in many papers [25] [26].

The SMC objective is to force the states of a system to slide on a given surface in the state space (sliding surface). If this limits the dynamics of the system to rest on a well-behaved surface, then the control problem can be greatly simplified. The surface is called the sliding surface and is defined such that the dynamics error is exponentially stable when the system is constrained to rest on this surface. Therefore, the control problem is reduced to driving the system over that surface and then ensuring that it stays on that surface all the time. The sliding surface S is defined by the following relation:

$$s = \left(\frac{\partial}{\partial t} + \boldsymbol{\lambda}\right)^{n-1} e \qquad (15)$$

where λ is the design parameter and is selected such that (λ > 0) to ensure sliding mode stability, and n is the order of the system. The current error is defined according to the following relationship:

$$e = i_{jref} - i_j \qquad (16)$$

By developing equation (16) in the case of a sliding mode control of order 2 ($n = 2$), we obtain the following relation:

$$s = \frac{\partial e}{\partial t} + \lambda e \qquad (17)$$

The objective of the sliding mode command is to minimize the surface S and its derivative $\dot{S}$. By substituting the equation (16) in (17) we have:

$$S = \left(\frac{\partial i_{jref}}{\partial t} - \frac{\partial i_j}{\partial t}\right) + \lambda\left(i_{jref} - i_j\right) \qquad (18)$$

Since the objective is to obtain $S = 0$ at all times, we then have:

$$\left(\frac{\partial i_{jref}}{\partial t} - \frac{\partial i_j}{\partial t}\right) + \lambda\left(i_{jref} - i_j\right) = 0 \qquad (19)$$

From relation (19), we obtain the dynamics phase currents as a function of parameter λ of the sliding surface:

$$\frac{\partial i_j}{\partial t} = \frac{\partial i_{jref}}{\partial t} + \lambda\left(i_{jref} - i_j\right) \qquad (20)$$

By making an equalization of equation (20) with relation (9), we obtain the equivalent command given by the following relation:

$$Ueq_j = \left[\frac{\partial i_{jref}}{\partial t} + \lambda\left(i_{jref} - i_j\right)\right]\left(\frac{\partial \psi_j(\theta, i_j)}{\partial i_j}\right) + R_s i_j + \frac{\partial \psi_j(\theta, i_j)}{\partial \theta}\,\Omega \qquad (21)$$

To obtain the sliding mode, the output of the sliding mode controller should be chosen as follows

$$U_j = U_{eq_j} + K.sign(S) \qquad (22)$$

To ensure a good dynamic response of the system, it is important to choose the right values of the parameters λ et K. In this work, we will use Particles Swarms optimisation (PSO) algorithm to obtain the optimal values of these parameters able to force the sliding surface to tend to zero.

The particle swarm optimization algorithm PSO (Particle Swarm Optimization) is one of the evolutionary type stochastic methods. This method is inspired by the behaviour of groups of animals in nature and its principle is based on collaboration between individuals to explore a specific area. Each individual who is part of the population (swarm) contributes with his experience to the evolution of the group and he uses the overall experience of the group for his own evolution. Thus, information passes in both directions, from the group to the individual and from the individual to the group [27].

The particle swarm algorithm is an iterative algorithm; at each calculation of step, individual's values are compared according to the fixed objective function and then the new guides are chosen. During its execution, the algorithm goes through the steps grouped in the following flowchart:

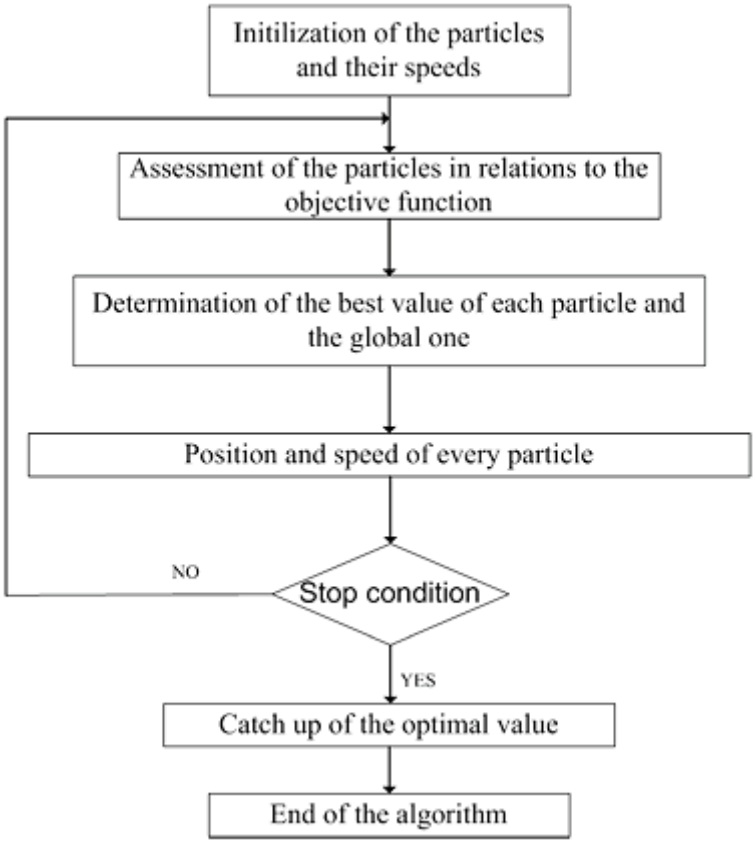

Figure 7: Flow chart of execution of PSO algorithm

The update of the position and the speed of each particle is carried out by application of the following equations

$$\begin{cases} V_{i+1} = \gamma_1 V_i + \gamma_2 (x_{ip} - x_i) + \gamma_p (x_g - xi) \\ x_{i+1} = x_i + V_{i+1} \end{cases} \quad (23)$$

With $\gamma_1, \gamma_2, \gamma_p$ values between 0 and 1, and chosen randomly; x_{ip} and x_g respectively the best position of a particle i since the first iteration, and the best global position of the swarm.

The application of PSO algorithm requires the choice of an objective function and parameters to be optimized with constraints not to be exceeded. In our case, we will optimize sliding mode controller parameters namely λ and K in order to reduce the torque error and to minimize the torque ripples. We therefore have to deal with a multi-objective optimization. Let T_r the torque ripple rate and J_I the integral of the quadratic error committed on the torque. The objective function can therefore be formulated by the following relation:

$$J_{ITAE} = \alpha T_r + \beta J_I \quad (24)$$

With α and β the weighting coefficients chosen respecting the following constraint:

$$\alpha + \beta = 1 \quad (25)$$

In this work, we chose $\alpha = \beta = 0{,}5$. The curve in figure 8 shows the evolution of the objective function according to iterations. We notice that the algorithm converged quickly from the 10th iteration.

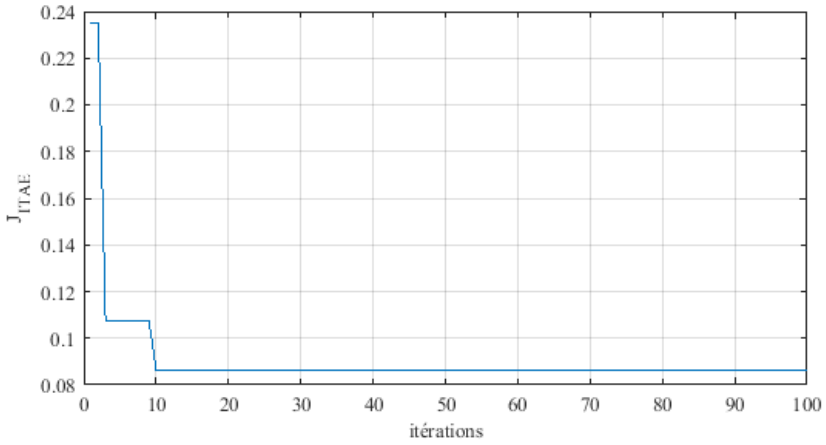

Figure 8: Evolution of the objective function

Figure 9 shows the control block diagram of the proposed TSF-SMC-PSO

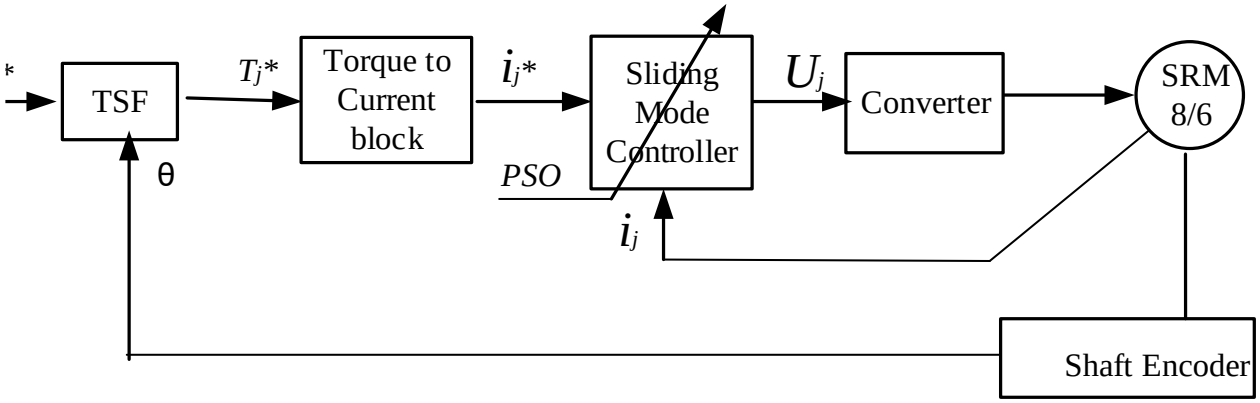

Figure 9: block diagram of TSF-SMC-PSO control

4.3. TSF-Sliding Mode-Fuzzy control (TSF-SMFC)

Many authors have proposed dynamic control reducing torque ripples using fuzzy logic control. This type of control is now well established in the field of control of electrical machines. Fuzzy logic control of a drive has been successfully implemented in [28] and found to be effective for speed control in applications where some degree of torque ripple is tolerated, such as the case in many industrial applications [29]. The fuzzy logic controller of a variable reluctance machine has been studied recently, to improve the performance of SRM in [28].

In this subsection, we will implement a fuzzy logic controller based on the torque sharing function method (TSF) associated with the sliding mode command. Indeed, in the sliding mode control exposed in the previous subsection, the parameter of the sliding surface (λ) and the parameter providing the sliding mode (K) have been optimized using the particle swarm algorithm (PSO). In this subsection, the slip parameter (K) will be obtained as a function of the current error and the dynamics of the current error noted respectively (e, ep) of each phase of SRM. Thus, on each phase

of the machine, the fuzzy controller that we have implemented has two inputs (the current error and its dynamics) and one output (the gain K of the sliding mode) as we can observe on the Simulink diagram of Figure 10.

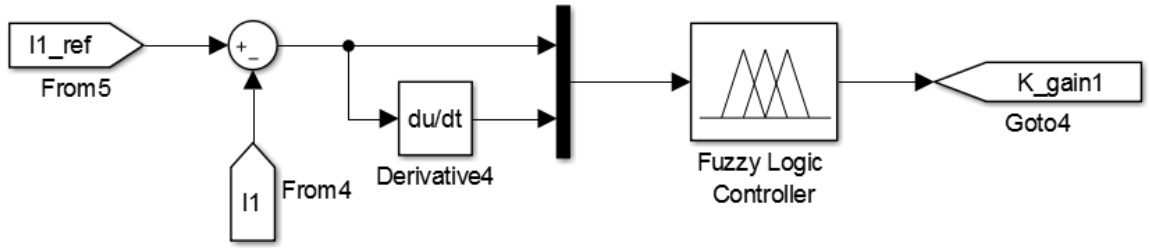

Figure 10: Simulink diagram block of Fuzzy logic control of the gain K

A fuzzy controller includes fuzzification process, knowledge base and defuzzification process. The membership functions chosen for the two inputs and the output of the fuzzy controller are given in figures 11, 12 and 13 respectively for the current error, the dynamics of the current error and the output. According to figures 11, 12 and 13, each membership function has seven fuzzy sets which are: negatives large (NL), negatives medium (NM), negatives small (NS), zero (Z), positives small (PS), positives medium (PM) and positives large (PL). The linguistic rule bases for the proposed fuzzy controller are presented in Table 3. The Mamdani type is used for the fuzzy inference system and the defuzzification type is bisector like use in [30].

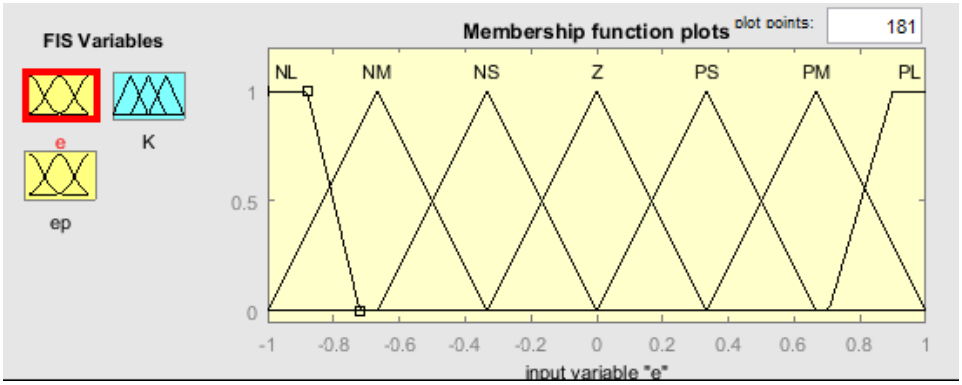

Figure 11 : input membership function of current error e

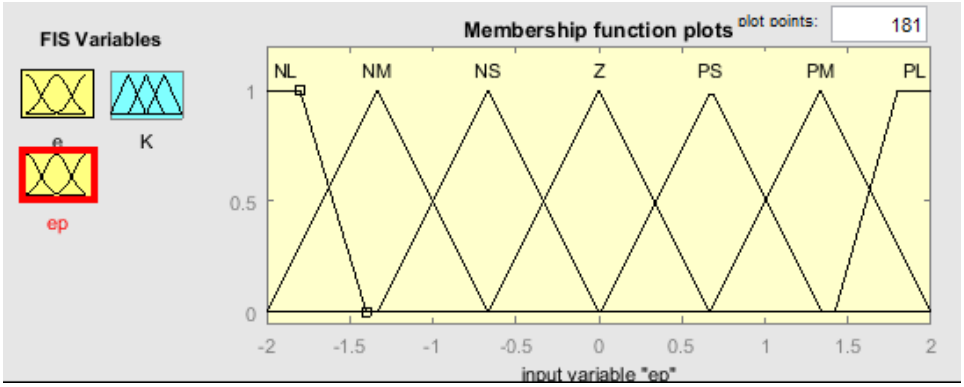

Figure 12 : input membership function of dynamic of current error e_p

Technium Vol. 4, No. 9 pp.23-46 (2022)
ISSN: 2668-778X
www.techniumscience.com

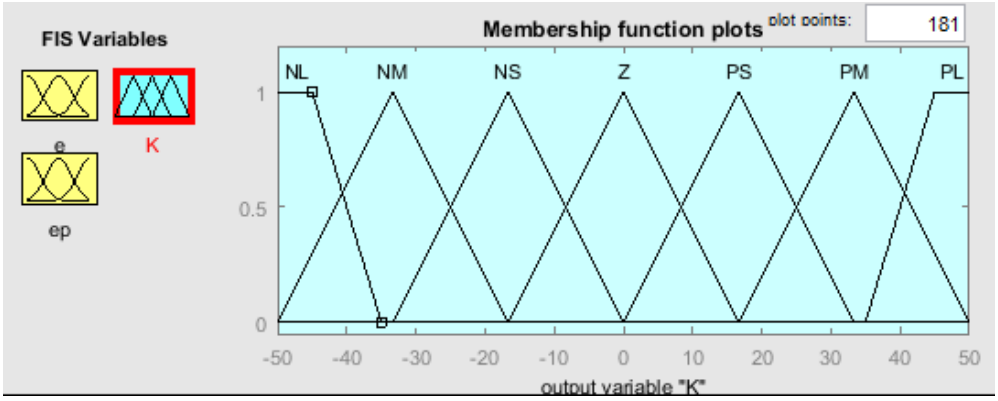

Figure 13: Output membership function of the gain *K*

Tableau 3**.** linguistic rule bases for the proposed fuzzy controller

e/e_p	NL	NM	NS	Z	PS	PM	PL
NL	NL	NL	NL	NL	NM	NM	Z
NM	NL	NL	NL	NM	NM	Z	PS
NS	NL	NL	NM	NM	Z	PS	PM
Z	NL	NM	NS	Z	PS	PM	PL
PS	NM	NS	Z	PS	PM	PL	PL
PM	NS	Z	PS	PM	PL	PL	PL
PL	Z	PS	PM	PL	PL	PL	PL

The surface viewer of the input variables (e, e_p) and the output variable (K) is shown in Figure 14. This surface viewer is used to show the dependence of the output variable on input variables. The output of the proposed FLC is used to generate the value of the gain K of the sliding mode controller for the command of SRM.

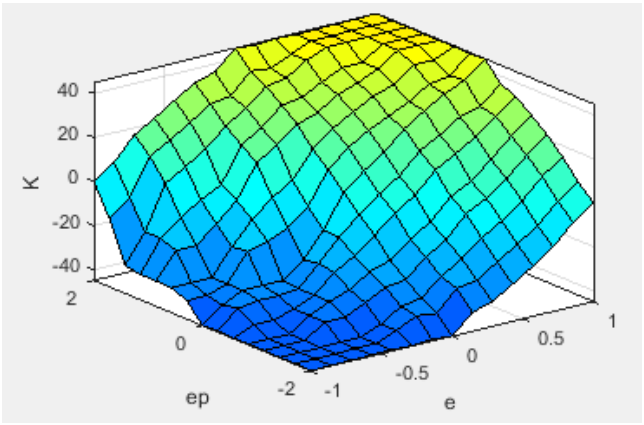

Figure 14: Surface view of the evolution of the gain K according to the input variables

The block diagrams of the implementation of this controller and the Simulink diagram are given in figures 15.

Technium Vol. 4, No. 9 pp.23-46 (2022)
ISSN: 2668-778X
www.techniumscience.com

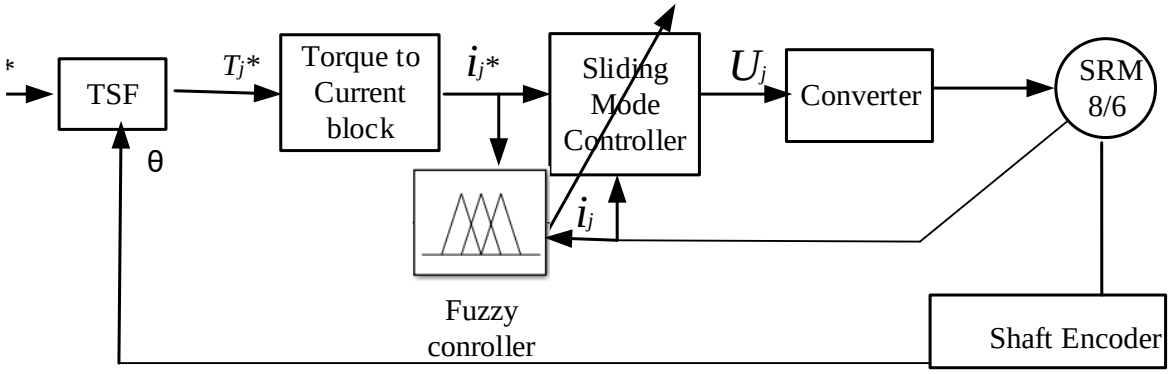

Figure 15: Block diagram of TSF-SMFC

These TSF models will be used in all the control approaches presented in this work. Besides, the parameters that we will evaluate in all the models are the torque ripple rate T_r and the average torque T_{av}. The Torque Ripple Rate can be expressed in percentage as follows [31] [32] :

$$T_r = \frac{T_{max} - T_{min}}{T_{avg}} * 100\ \% \qquad (26)$$

Where T_{max} is maximal torque; T_{min} is minimal torque; and T_{avg} the mean torque.

5. Simulation Results and Discussions

In order to highlight the performance of various control techniques developed in this work, we simulate the dynamic behavior of the studied SRM by applying each control techniques while taking into account the data obtained from the finite element analysis in order to taking into account the magnetic saturation of the circuit.

The study of the dynamic behavior of 8/6 SRM will be done in two stages. First, we will present the results of the dynamic behavior of the motor without external disturbances; then, we will carry out the tests of robustness of the various proposed technics.

5.1. Dynamics response of 8/6 SRM

Curves in figure 16 present respectively the curves of currents per phase, the reference torque per phase, the torque produced per phase and finally the total electromagnetic torque. In figure 16.a we have the results obtained by the TSF-H method and in figure 16.b the results obtained by the TSF-P method.

Similarly, Curves in figure 17.a present the results obtained by the TSF-SMFC method and in figure 17.b the results obtained by the TSF-SMC-PSO method.

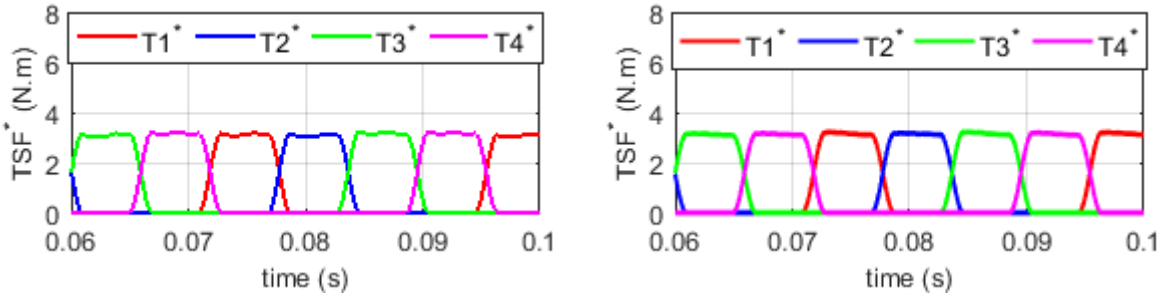

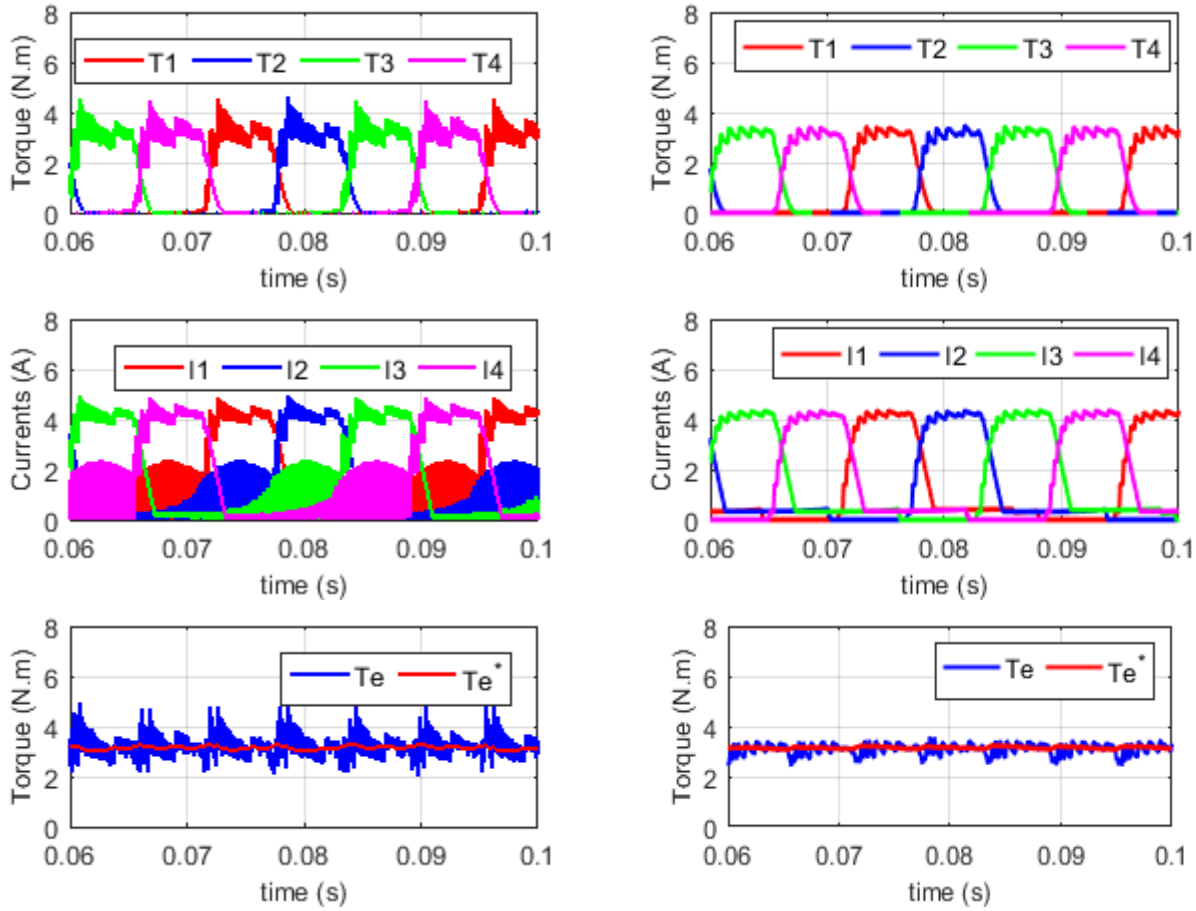

(a) (b)

Figure 16: Dynamic behavior simulation results: (a) TSF-H control; (b) TSF-P control.

Observation of the results in figure 17 clearly show that the torque control method using TSF, associated with the controller by hysteresis (TSF-H) presents a torque response with a large ripple although the pace oscillates around the reference; moreover, the response of the phase currents shows strong oscillations, especially before switching between the phases; which produces a residual torque which justifies the strengthening of the torque ripples. On the other hand, the TSF-P method presents an improved response of the torque compared to that by TSF-H.

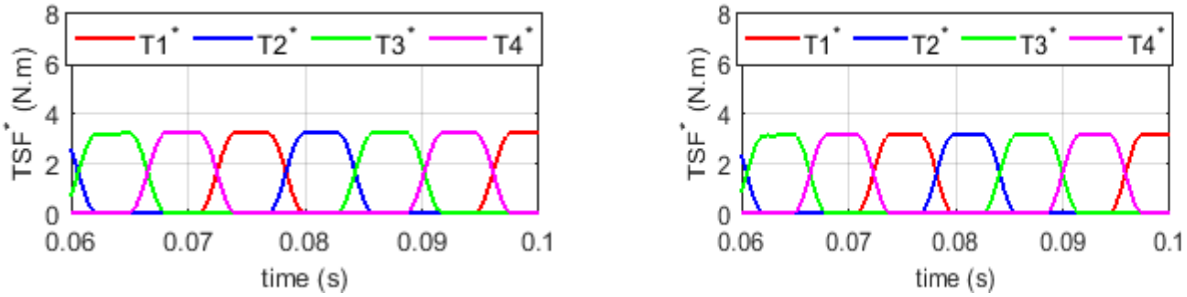

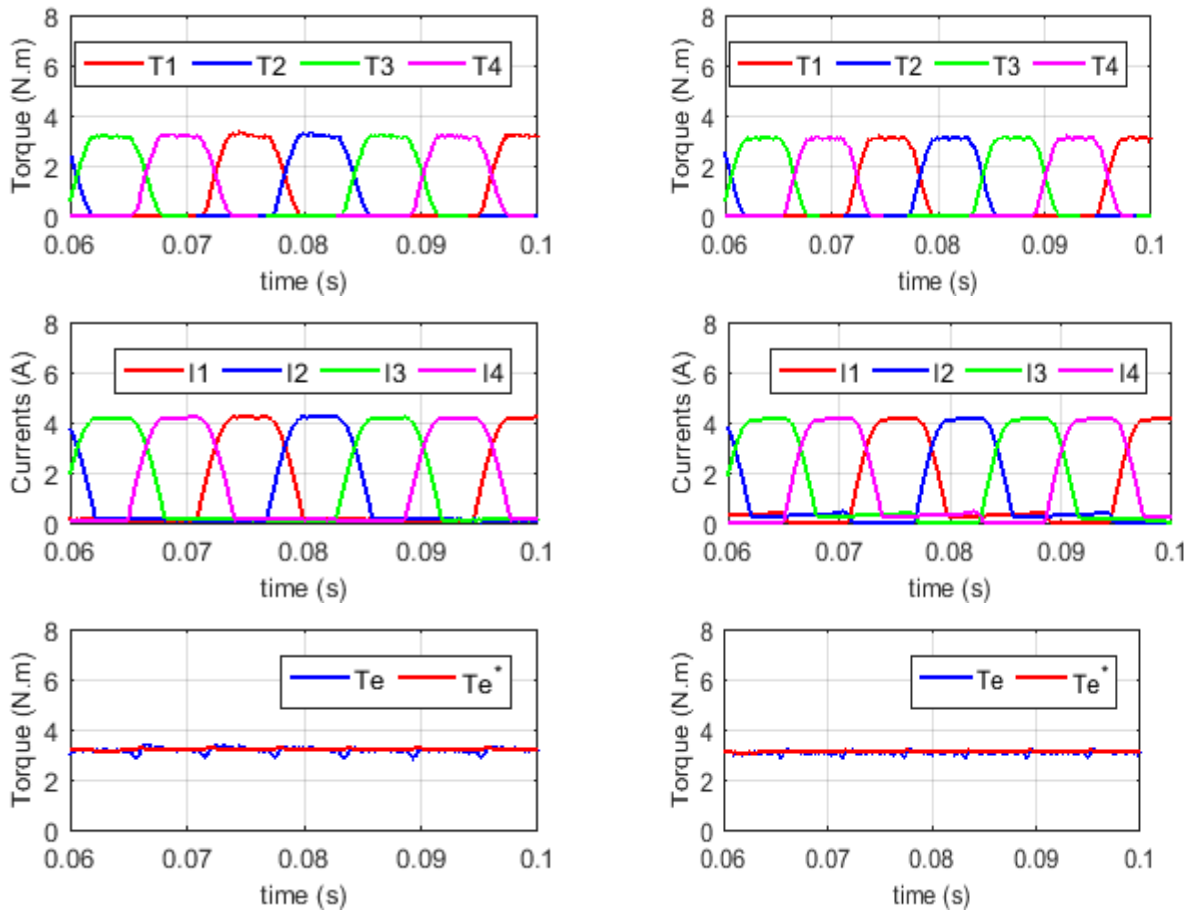

(a) (b)

Figure 17: Dynamic behavior simulation results: (a) TSF-SMFC; (b) TSF-SMC-PSO.

The results of figure 17 show that the TSF-SMC-PSO method gives a result of the total electromagnetic torque produced by the motor with oscillations slightly lower than that obtained by the TSF-SMFC method. Furthermore, the other performance quantities (phase currents, polyphase torques) give almost similar appearances for the two methods. In qualitative comparison with the other methods whose answers are exposed previously, we can conclude that these two methods present better results. In order to better appreciate the dynamic performance of these control methods, we have summarized in Table 4, the maximum torque, the minimum torque, the average torque and the torque ripple rate for these differents control methods.

Table 4: Summary of the performances of the different methods exposed

	TSF-H	**TSF-P**	**TSF-SMFC**	**TSF-SMC-PSO**
$\boldsymbol{T_{max}}$**(N.m)**	4.9783	3.6293	3.4045	3.2032
$\boldsymbol{T_{min}}$ **(N.m)**	2.0434	2.4810	2.8178	2.8343
$\boldsymbol{T_{avg}}$ **(N.m)**	3.2078	3.1152	3.1735	3.0685
$\boldsymbol{T_r}$ (%)	89.62	36.86	18.49	**12.02**

Observation of Table 4 shows that the TSF-SMC-PSO method has a low ripple rate of 12.02 % compared to other methods, although having an average torque slightly lower than the other methods (3. 0685 N.m against 3.2078 N.m for the TSF-H control, 3. 1152 N.m for the TSF-P control, 3. 1735N.m for the TSF-SMFC). Moreover, the TSF-H method presents a performance in terms of very high torque ripple. Indeed, this method requires a large calculation step while the other methods presented (TSF-P, TSF-SMFC, TSF-SMC-PSO) give an interesting answer with a low calculation time, which makes them suitable for a study and control with rapid acquisition in real time with the aim of reducing torque ripples and therefore acoustic noise in the motor.

5.2. Robustness tests of the control approaches adopted

In order to highlight the performance of the TSF-P, TSF-SMFC, TSF-SMC-PSO controllers in the face of external disturbances rejection which may occur in the dynamic behavior of the motor, we will in the rest of this work carry out the variations of certain parameters of the dynamic model of the machine such as the phase resistance (R), the moment of inertia (J) and the coefficient of friction (f_v) and this under the same supply conditions.

5.2.1. Robustness test against phase resistance variation. The dynamic behavior of the motor under the variation of the phase resistance is presented in this subsection. At time $t = 0.1s$, the phase resistance is increased by 25% of its initial value. The simulation results are presented in Figures 18 for the three methods used.

We note from these curves that the increase in the resistance of the phases has a slight influence on the torque response obtained for the three methods used (figure 18). This statement is confirmed by comparing the performance data summarized in Table 4 to the performance data presented in Table 5. The influence is even less slight for the TSF-SMC-PSO method than for the other methods. This means that this controller better rejects disturbances on the resistance of the phases.

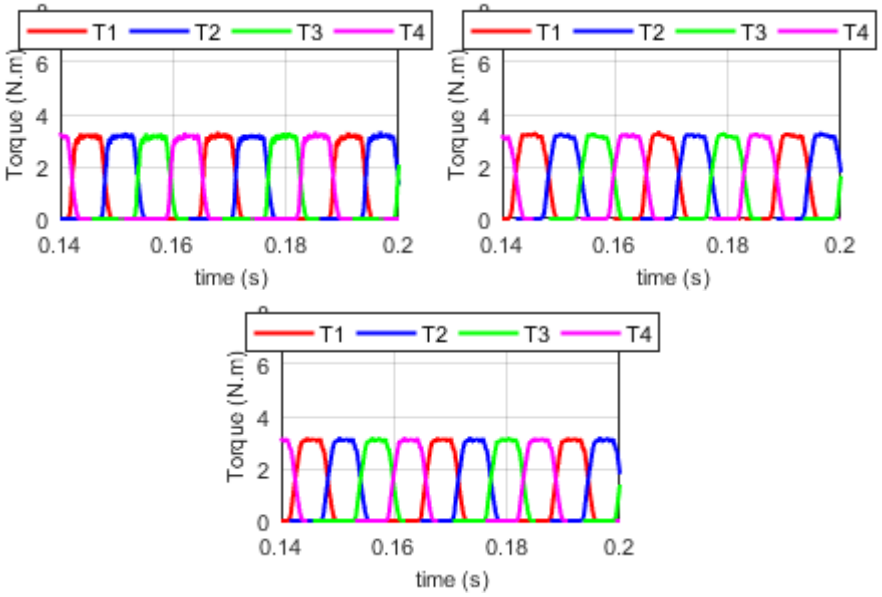

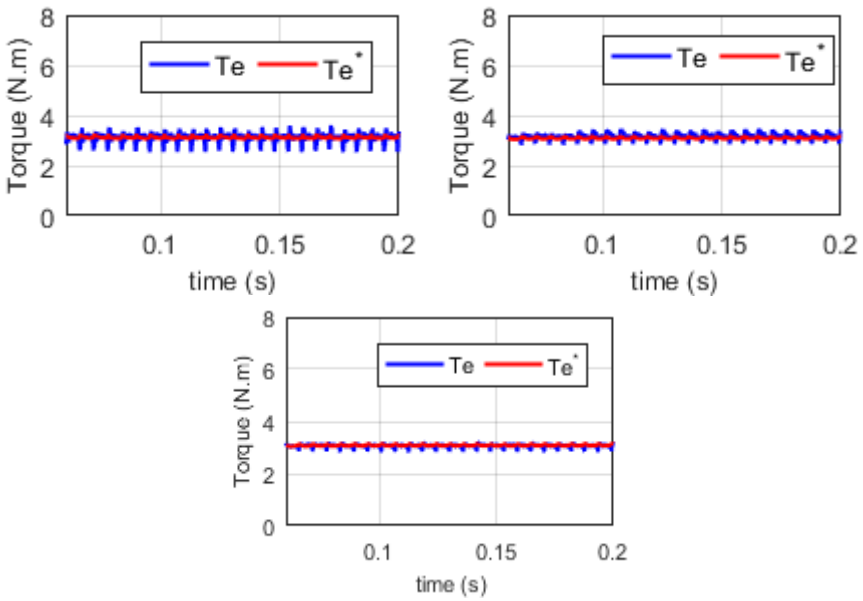

(a) (b) (c)

Figure 18: Variation of 25% of the phases résistance R :
(a) TSF-P; (b) TSF-SMC; (c) TSF-SMC-PSO.

Tableau 5 : Résultats des tests de robustesse sous augmentation de 25% de la résistance des phases R

	TSF-P	**TSF-SMFC**	**TSF-SMC-PSO**
$\boldsymbol{T_{max}}$**(N.m)**	3.6075	3.4530	3.2121
$\boldsymbol{T_{min}}$ **(N.m)**	2.5305	2.8552	2.8339
$\boldsymbol{T_{avg}}$ **(N.m)**	3.1152	3.1925	3.0672
$\boldsymbol{T_r}$ (%)	34.57	18.72	**12.32**

5.2.2. Test of robustness against the variation of the moment of inertia. As for the case of the resistance of the phases, we make a sudden increase of 25% of the moment of inertia always at the moment $t = 0.1s$. The results of simulations are presented in figure. 19 From these results, the same remarks presented previously are observed.

Indeed, the variation of the moment of inertia of the motor has a weak influence on the behavior of this one for all the exposed controllers. We note once again a good performance of the TSF-SMC-PSO control approach compared to the other approaches, especially in terms of maintaining the torque ripples at a low value in comparison with the results in Table 6 with those obtained in the absence of disturbances presented in Table 4.

Technium Vol. 4, No. 9 pp.23-46 (2022)
ISSN: 2668-778X
www.techniumscience.com

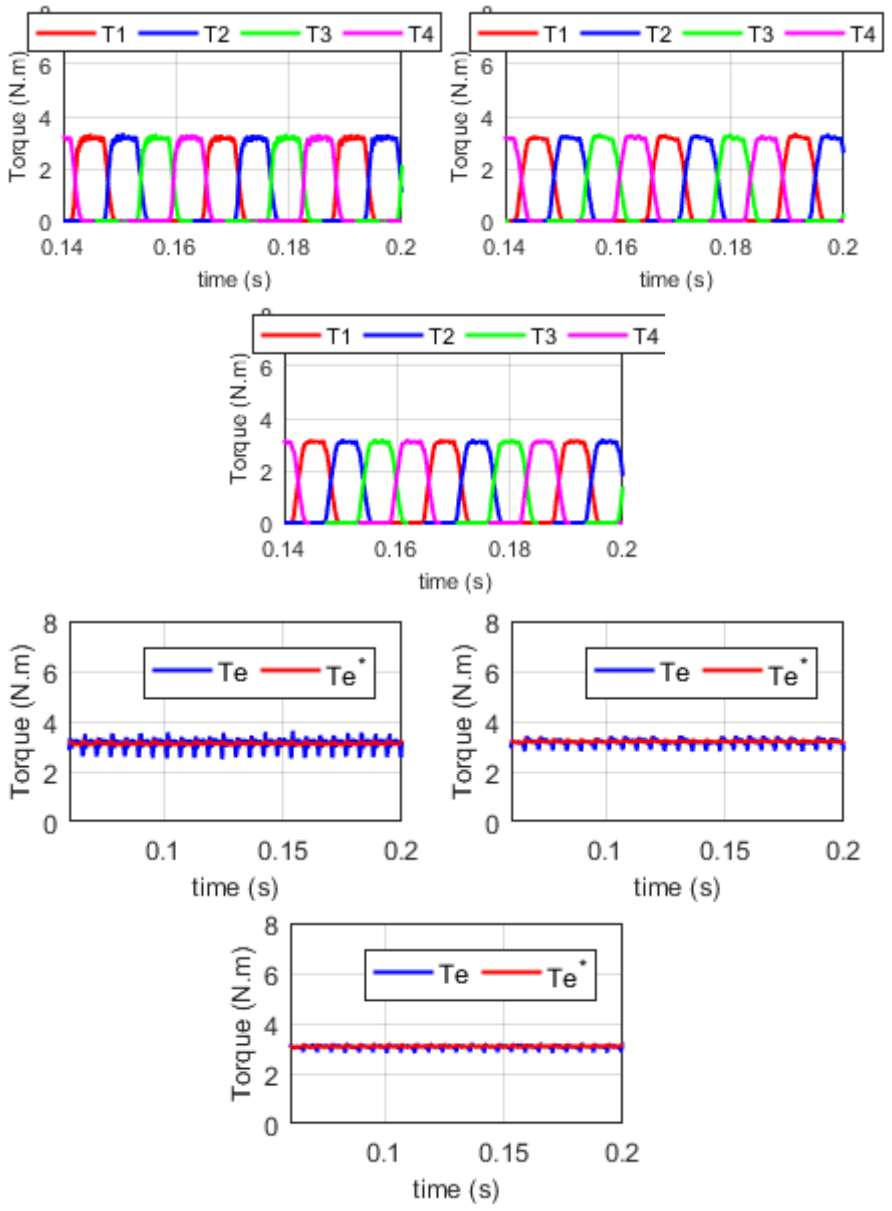

(a) (b) (c)

Figure 19 : Variation of 25% moment of inertia J:
(a) TSF-P; (b) TSF-SMC; (c) TSF-SMC-PSO.

Tableau 6 : Result of robustness test under variation of 25% moment of inertia J

	TSF-P	**TSF-SMFC**	**TSF-SMC-PSO**
$\boldsymbol{T_{max}}$**(N.m)**	3.6248	3.4407	3.2135
$\boldsymbol{T_{min}}$ **(N.m)**	2.4936	2.8104	2.8371
$\boldsymbol{T_{avg}}$ **(N.m)**	3.1170	3.1829	3.0707
$\boldsymbol{T_r}$ (%)	36.29	19.80	**12.25**

5.2.3. Test of robustness by variation of the coefficient of friction. The results in figure 20 show the dynamics of the machine when the coefficient of friction f_v suddenly increases by 25% of its initial value at $t = 0.1s$. Once again these results show that the effect of the sudden variation of the friction coefficient was rejected by the three controllers implemented since it has a weak influence on the dynamic performance quantities of the machine. Observation of Table 7 shows that the TSF-SMC-PSO method presents a result in terms of torque ripple almost unchanged, which once again puts this method ahead of the other control approaches exposed in this work.

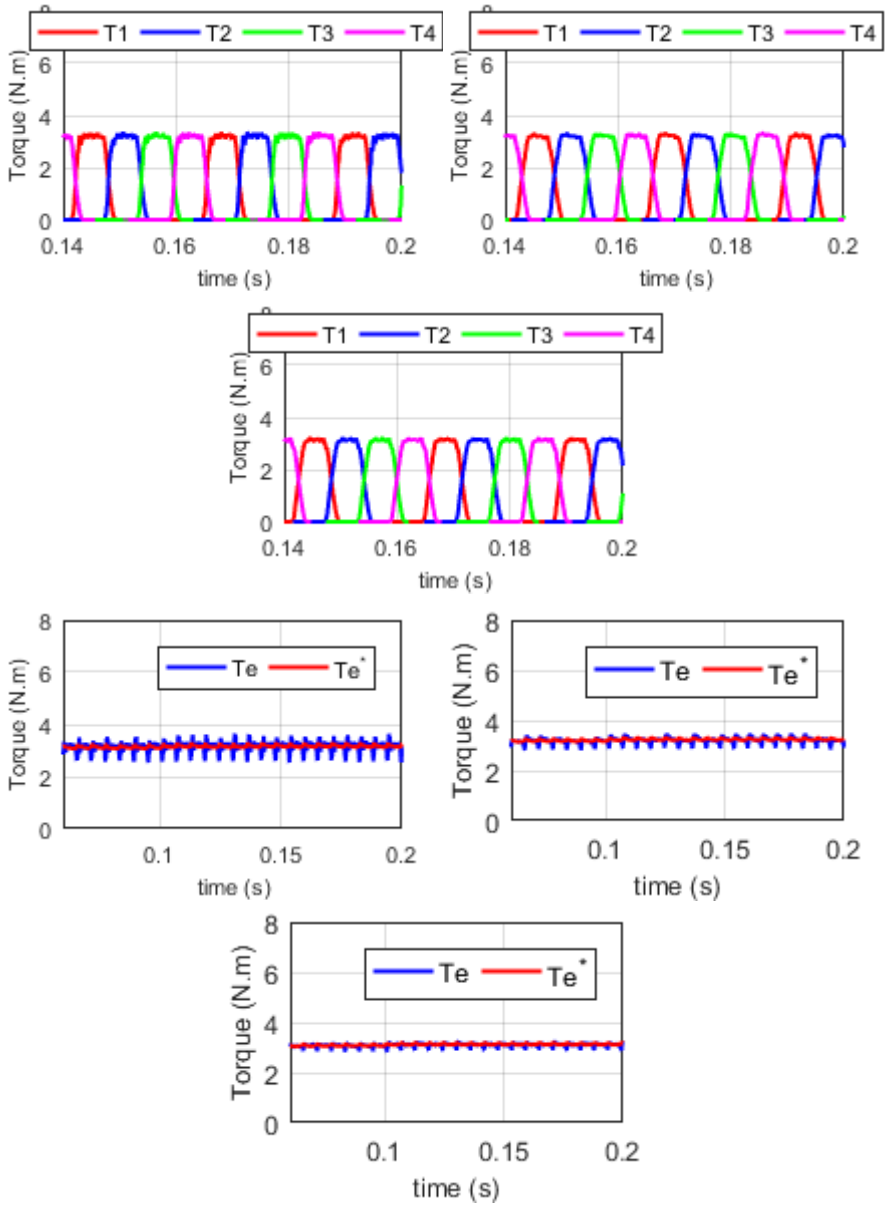

(a) (b) (c)

Figure 20 : Variation of 25% the coefficient of friction f_v:
(a) TSF-P ; (b) TSF-SMC ; (c) TSF-SMC-PSO.

Tableau 7 : Result of robustness test under variation of 25% coefficient of friction f_v

	TSF-P	**TSF-SMFC**	**TSF-SMC-PSO**
$\boldsymbol{T_{max}}(\mathbf{N.m})$	3.6544	3.4834	3.2590
$\boldsymbol{T_{min}}$ $(\mathbf{N.m})$	2.5298	2.8642	2.8815
$\boldsymbol{T_{avg}}$ $(\mathbf{N.m})$	3.1591	3.2185	3.1127
$\boldsymbol{T_r}$ (%)	35.59	19.23	**12.12**

In view of all the results presented in this work, it is clear that the control approach that we named TSF-SMC-PSO presents a better result with a lower torque ripple than for the other approaches. In addition, robustness tests against variations of certain parameters of the dynamic model of the machine have shown that, although the TSF-P and TSF-SMFC methods present results with a weak influence of these disturbances, the TSF-SMC-PSO has a better response in terms of disturbance rejection.

6. Conclusion

In this work, some control techniques of a variable reluctance machine with minimization of torque ripples have been studied. The finite element method analysis technique was used to calculate the characteristic quantities of the static behavior of the variable reluctance machine taking into account the geometric structure and the saturation of the magnetic circuit; then, the results of the static calculation are integrated into the dynamic model of the machine. The torque control approach by the sharing function method is used and associated with the various techniques for reducing the torque ripples investigated. These techniques were, among others: the TSF-Hysteresis control method (named TSF-H), the TSF-Predictive control method (named TSF-P), the TSF-Sliding Mode-Fuzzy control method (named TSF-SMFC) and the TSF-Sliding Mode-PSO control method (named TSF-SMC-PSO). The stochastic optimization method by particle swarm algorithm was used for the calculation of the optimal values of the parameters sliding mode controller that forcing the torque dynamics to follow its reference with a low ripple rate. The simulations carried out in the Matlab/Simulink environment showed that the TSF-H method presents strong torque ripples compared to the other methods. Moreover, the calculation of performance quantities such as the average torque and the torque ripple rate shows that the TSF-SMC-PSO method is the most efficient. The robustness tests have once again proven that this method effectively rejects the disturbances that may occur on the parameters of the dynamic model. In perspective to this work, we will perform an optimization of the proposed controller by taking into account the torque and speed profile in electric traction.

Nomenclature

Ω : angular rotor speed.

J : moment of inertia

θ : rotor position

ψ_j : flux linkage of j^{th} phase

i_{jk} : discretized current j^{th} phase

U_{jk} : discretized voltage j^{th} phase

ψ_{jk} : discretized flux linkage j^{th} phase

i_j ; current of j^{th} phase

U_j : voltage of j^{th} phase

R_s : resistance phase of stator

f_v : friction coefficient

T_e : electromagnetic torque

T_j : torque of j^{th} phase

T_s : calculation step

T_r : torque ripple rate

T_{max} : maximal torque

T_{min} : minimal torque

T_{avg} : average torque

j = 1, 2, 3, 4

$Tj\ Ref$: reference torque of j^{th} phase

$ij\ Ref$: reference current of j^{th} phase

$\frac{\partial \psi_j(\theta, i_j)}{\partial \theta}$: back emf per unit speed.

$\frac{\partial \psi_j(\theta, i_j)}{\partial i_j}$: incremental inductance

REFERENCES

[1] A. Chithrabhanu et K. Vasudevan, «Online Compensation for Torque Ripple Reduction in SRM drives,» *IEEE Transportation Electrification Conference India*, vol. 1, n° %19, pp. 978-986, 2017.

[2] T. Miller, «Optimal design of switched reluctance motors,» *IEEE trans. Ind Electron*, vol. 49, n° %11, pp. 15-17, 2002.

[3] B. Bilgin, A. Emadi et Krishnamurthy, «Design considerations for switched reluctance machine with a high number of rotor poles,» *IEEE Trans. Ind. Electon.*, vol. 59, pp. 3745-3756, Oct 2013.

[4] H. Li, B. Bilgin et A. Emadi, «An Improved Torque Sharing Function for Torque Ripple Reduction in Switched Reluctance Machines,» *IEEE Transactions on Power Electronics*, 2018.

[5] a. Li, «Comparative Studies between Classical and Mutually Coupled Switched Reluctance Motors using Thermal-Electromagnetic Analysis for Driving Cycles,» *IEEE Transaction on magnetic*, vol. 47, n° %14, pp. 839-847, April 2011.

[6] C. Gan, J. Wu, Q. Sun et Wubin Kong, «A Review on Machine Topologies and Control Techniques for Low-Noise Switched Reluctance Motors in Electric Vehicle Applications,» *IEEE trans*, 2018.

[7] I. Husain, «Minimization of torque ripple in SRM drives,» *IEEE Transactions on Industrial Electronics,* vol. 49, n° %11, pp. 28-39, feb 2002.

[8] Doncker, K. T et R. W. De, «Optimal torque sharing in direct instantaneous torque control of switched reluctance motors,» *IEEE Energy Conversion Congress and Exposition,* n° %11, pp. 327-333, 2015.

[9] V. P. Vujicic, «Minimization of torque ripple in switched reluctance motor drives,» *IEEE Trans. Power Electron,* vol. 27, n° %11, pp. 388-399, jan. 2012.

[10] J. Ye, B. Bilgin et A. Emadi, «An offline torque sharing function for torque ripple reduction in switched reluctance motor drives,» *IEEE Trans. Energy Convers.,* vol. 30, n° %12, pp. 726-735, jun 2015.

[11] S. K. Sahoo, S. K. Panda et J.-X. Xu, «Indirect torque control of switched reluctance motors using iterative learning control,» *IEEE Transactions on Power Electronics,* vol. 20, n° %11, pp. 200-208, 2005.

[12] M. Dowlatshahi, Nejad et Ahn, «Torque ripple minimization of switched reluctance motor using modified torque sharing function,» *in 2013 21st Iranian Conference on Electrical Engineering,* pp. 1-6, 2013.

[13] D. H. Lee, J. Liang, Z. G. Lee et a. J. W. Ahn, «A simple nonlinear logical torque sharing function for low-torque ripple SR drive,» *IEEE Trans. Ind. Electron,* vol. 58, n° %18, pp. 3021-3028, Aug 2009.

[14] S. Sahoo, S. Panda et J. Xu, «Indirect torque control of switched reluctance motors using iterative learning control,» *IEEE Trans. Power Electron.,* vol. 20, n° %11, pp. 200-208, Jan 2015.

[15] R. Mikail, I. Husain, Y. Sozer, M. S. Islam et T. Sebastian, «Torque ripple minimization of switched reluctance machines through current profiling,» *IEEE Trans. Ind. Appl.,* vol. 49, n° %13, pp. 1258-1267, May 2013.

[16] C. Labiod, K. Srairi, B. Mahdad, M. T. Benchouia et M. Benbouzid, «Speed control of 8/6 switched reluctance motor with torque ripple reduction taking into account magnetic saturation effects,» *Elsevier,* vol. 74, pp. 112-121, 2015.

[17] Farah et Nabil, «Multilevel Inverter Fed Switched Reluctance Motors (SRMs) 6/4, 8/6 and 10/8 SRM Geometric Types,» *International Journal of Power Electronics and Drive System,* vol. 8, n° %12, pp. 584-592, 2017.

[18] A. D. Tellapati et M. K. Kumar, «A simplified hysteresis current control for cascaded converter fed switched reluctance motor,» *International Journal of Electrical and Computer Engineering,* vol. 9, n° %16, pp. 5095-5106, December 2019.

[19] N. Farah, J. Bt, M. Lazi et M. Talib, «Comparative Study of Three Different Topologies of Five-level Inverter with SPWM Modulation Technique,» *International Journal of Power Electronics and Drive System,* vol. 8, n° %14, p. 1612~1621, December 2017.

[20] Y. Qin, C. He, X. Shao, H. Du et C. Xiang, «Vibration mitigation for in-wheel switched reluctance motor driven electric vehicle with dynamic vibration absorbing structures,» *Journal of Sound and Vibration,* pp. 249-267, 2018.

[21] Y. Wei, M. Qishuang, Z. Poming et G. Yangyang, «Torque Ripple Reduction in Switched Reluctance Motor Using a Novel Torque Sharing Function,» *IEEE/ International Conference on Aircraft Utility Systems (AUS),* 2016.

[22] Vasudevan, Krishna et A. Chithrabhanu, «Online Compensation for Torque Ripple Reduction in SRM drives,» *IEEE Transportation Electrification Conference,* 2017.

[23] J. Cai et Z. Deng, «A Position Sensorless Control of Switched Reluctance Motors Base on phase inductance Slope,» *Journal of Power Electronics,* vol. 13, n° %12, 2013.

[24] Buja, Menis et Valla, «Variable structure control of a SRM drive,» *IEEE Trans. Industrial Electron.,* vol. 40, n° %11, pp. 56-63, febuary 1993.

[25] M. K. A. S. K. Erbatur, « A study on robustness property of sliding mode controllers: a novel

design and experimental investigations,» *IEEE Trans. Industrial Electron*, vol. 46, n° %15, pp. 1012-1017 , October 1999 .

[26] Sabanovic, Jezernik et Wada, «Chattering free sliding modes in robotic manipulators control,» *Robotica*, vol. 14, pp. 17-29, 1996.

[27] I. Dan, «Conception optimale des moteurs à réluctance variable à commutation électronique pour la traction des véhicules électriques légers,» *Thèse de Doctorat de l'Ecole Centrale de Lille*, 25 Octobre 2011.

[28] Rodrigues, Suemitsu, Branco, Dente et Rolim, «Fuzzy Logic Control of a Switched Reluctance Motor,» *IEEE International Symposium on Industrial Electronics*, pp. 527-531, 1997.

[29] Greenhough, «Switched Reluctance Variable Speed Drives- A Focus on Aplications,» *Technology Mining - Papers and articles ,,* pp. 107-110, Abril 1996.

[30] Beromi, Z. Moravej et S. Darabi, «Torque Ripple Reduction of Switched Reluctance Motor Using PID Fuzzy Logic Controller,» *International Conference and Exposition on Electrical and Power Engineering*, 2012.

[31] C. Ma et L. Qu, vibration and torque ripple reduction of switched reluctance motor through current profile optimazation, USA: IEEE, 2016.

[32] A. Chithrabhanu et a. K. Vasudevan, «Online Compensation for Torque Ripple Reduction in SRM drives,» *IEEE Transportation Electrification Conference (ITEC-India)*, vol. 978, n° %11, pp. 5386-2668, 2017.